AIAA 91-1469

ELECTROHYDRODYNAMIC (EHD) FLOW MODELING AND COMPUTATIONS

Seungsoo Lee
Agency for Defense Development
Daejon, South Korea

George S. Dulikravich and Branko Kosovic
The Pennsylvania State University
University Park, PA 16802, USA

AIAA 22nd Fluid Dynamics, Plasma Dynamics & Lasers Conference
June 24-26, 1991 / Honolulu, Hawaii

ELECTROHYDRODYNAMIC (EHD) FLOW MODELING AND COMPUTATIONS

Seungsoo Lee[1], George S. Dulikravich[2], and Branko Kosovic[3]
Department of Aerospace Engineering, 233 Hammond Building
The Pennsylvania State University, University Park, PA 16802

Abstract

A complete system of partial differential equations governing three-dimensional laminar flow of an incompressible viscous neutrally charged carrier fluid injected with an electrically charged fluid has been elaborated. The model accounts for temperature dependent physical properties via an extended Boussinesq approximation while including a Joule heating effect. The system of coupled partial differential equations was solved using an artificial compressibility formulation and explicit finite differencing with a four-step Runge-Kutta time integration. Two-dimensional numerical results demonstrate a case of an electrohydrodynamic instability and several cases of bending of a stream of charged particles under the influence of an external electric field. Transformation of an initially circular domain of charged particles into oval and crescent shapes was also demonstrated with success.

Nomenclature

$\tilde{A}$	= ξ-flux vector Jacobian in curvilinear nonorthogonal coordinates
AR	= aspect ratio (length/height)
b	= charged particles mobility coefficient [$m^2\ s^{-1}\ V^{-1}$]
$\tilde{B}$	= η-flux vector Jacobian in curvilinear nonorthogonal coordinates
c_p	= specific heat coefficient [$m^2\ K^{-1}\ s^{-2}$]
$\tilde{C}$	= ζ-flux vector Jacobian in curvilinear nonorthogonal coordinates
D	= diffusivity of charged particles [$m^2\ s^{-1}$]
D	= differential operator
D	= diagonal matrix
E	= electric field vector [$V\ m^{-1}$]
E_x, E_y, E_z	= x, y and z component of the electric field vector
E	= x-flux vector in Cartesian coordinates
$\tilde{E}$	= ξ-flux vector in curvilinear nonorthogonal coordinates
F	= y-flux vector in Cartesian coordinates
$\tilde{F}$	= η-flux vector in curvilinear nonorthogonal coordinates
g_{ij}	= metric tensor
g	= gravity force per unit volume [$N\ m^{-3}$]
G	= z-flux vector in Cartesian coordinates
$\tilde{G}$	= ζ-flux vector in curvilinear coordinates
J	= electric current per unit volume [$A\ m^{-3}$]
I	= identity matrix
k	= heat conductivity coefficient [$kg\ m\ s^{-3}\ K^{-1}$]
k_b	= Boltzman's constant [$kg^{-1}\ s\ K$]
l	= length [m]
L	= selection matrix (also latent heat)
M	= modal matrix
n	= unit vector normal to the solid wall
p	= pressure [$N\ m^{-2}$]
$\bar{p}$	= combined pressure [$N\ m^{-2}$]
q	= electric charge density per unit volume [$kg\ m^{-1}\ s^{-2}\ V^{-1}$]
$\tilde{R}$	= residual vector
Q	= solution vector in Cartesian coordinates
$\tilde{Q}$	= solution vector in curvilinear nonorthogonal coordinates

[1]Postdoctoral fellow, presently with Agency for Defense Development, Daejon, South Korea.
[2]Associate Professor. Associate Fellow AIAA.
[3]Graduate Student.

$\hat{R}$ = residual vector
S = source term vector in Cartesian coordinates
$\hat{S}$ = source term vector in curvilinear nonorthogonal coordinates
t = time [s]
T = temperature [K]
ΔT = temperature difference [K]
u, v, w = velocity components in Cartesian coordinates [m s^{-1}]
U, V, W = contravariant velocity components [m s^{-1}]
v = velocity vector in Cartesian coordinates [m s^{-1}]
x,y,z = Cartesian coordinates [m]
α = thermal expansion coefficient [K^{-1}]
β = artificial compressibility coefficient
δ = smoothing operator
ε = electrical permitivity coefficient [kg m s^{-2} V^{-2}]
ε_2 = second order artificial dissipation coefficient
ε_4 = fourth order artificial dissipation coefficient
$\hat{\Lambda}$ = eigenmatrix of a Jacobian flux vector
ξ,η,ζ = curvilinear coordinates [m]
η = viscosity coefficient [kg m^{-1} s^{-1}]
ω = smoothing coefficient for residual
Ω = boundary condition vector
ϕ = gravity potential [m^2 s^{-2}]
φ = electric potential [V]
ψ = artificial dissipation sensor function
ρ = fluid density [kg m^{-3}]
θ = nondimensional temperature difference

subscripts

c = cold wall
e = electrical
h = hot wall
o = reference values

superscripts

* = nondimensional values
T = transpose of a matrix

1. Introduction

This work is based on the fundamental paper by Stuetzer[1] who clearly delineated Magnetohydrodynamics (MHD) from Electrohydrodynamics (EHD) as representing two extreme models for a fluid flow under the influence of electromagnetic fields. The MHD model assumes that there are no charged particles in the flow field and that there is no electric potential applied. These types of flows have been discussed in a number of publications[2-4]. EHD on the other hand assumes that there is no magnetic field applied[1,5-9]. Instead, an external electric field is applied to an electrically conducting fluid containing electrically charged particles. These particles are convected with the flow field in the case when there is a mean flow. At the same time, the charged particles can diffuse and move[10-12] under the influence of the outside (imposed) and inside (self-induced) electric field. When modeling EHD flows, in addition to complete Navier-Stokes equations, one should add an equation for electric charge preservation for each of the electrically charged species[7,13]. One equation governing the electric potential field must also be added. In the momentum equation we will include a thermal buoyancy force using the extended Boussinesq approximation[14] and an electrical (Lorentz) body force[1,15]. In the energy equation we will add a Joule heating term[15], while neglecting viscous dissipation in accordance with the Boussinesq approximation. Although relatively well documented analytical models for EHD flows have been developed[1,5-9], somewhat incomplete versions of these models have been numerically solved[16-19] in the past.

The objective of this paper is to present a fully three-dimensional mathematical model, a numerical algorithm for its solution and computational results for cases of two-dimensional steady laminar EHD flows. The model consists of a neutral carrier fluid with a single species of charged fluid. This model can be easily extended to multi-species problems[7,13] including non-neutral carrier fluids.

2. Analytical model

The system of governing equations[1,15] is derived from a combination of Maxwell's equations of

electrodynamics and the Navier-Stokes equations. An idealized charged fluid is assumed and therefore magnetic fields can be neglected. Maxwell's equations reduce to a charge conservation equation and Poisson's partial differential equation for electric potential since in this case the electric field $\boldsymbol{E}$ is irrotational. It should be noted that the electric permitivity ε is assumed to be uniform. Thus, the governing equations are:

Continuity

$$\nabla \cdot \mathbf{v} = 0 \tag{1}$$

Momentum (including thermal buoyancy force and electric Lorentz force)

$$\rho_o \frac{D\mathbf{v}}{Dt} = -\nabla p - \rho_o \alpha g \Delta T + \nabla \cdot (\eta_o \nabla \mathbf{v}) + q\boldsymbol{E} \tag{2}$$

Energy (including Joule heating)

$$\rho c_p \frac{DT}{Dt} = \nabla \cdot (k \nabla T) + \mathbf{J} \cdot \boldsymbol{E} \tag{3}$$

Electric charge conservation

$$\frac{\partial q}{\partial t} + \nabla \cdot \mathbf{J} = 0 \tag{4}$$

Electric potential field

$$\nabla \cdot \boldsymbol{E} = \frac{q}{\varepsilon} \tag{5}$$

The induced electric current per unit volume is given by Ohm's law

$$\mathbf{J} = q(\mathbf{v} + b\boldsymbol{E}) - D \nabla q \tag{6}$$

The electric charge diffusivity coefficient D and mobility coefficient b are related by the Einstein's formula[7]

$$D = \frac{k_b T}{q\, m_i} \rho_i b \tag{7}$$

where m_i is the mass of a charged particle and ρ_i is the density of the non-neutral fluid. Since the electric field is irrotational, it follows that

$$\nabla \times \boldsymbol{E} = 0 \tag{8}$$

$$\boldsymbol{E} = -\nabla \varphi \tag{9}$$

where φ is the electric potential, so that equation (5) becomes

$$\nabla^2 \varphi = -\frac{q}{\varepsilon} \tag{10}$$

Nondimensionalization can be performed with respect to the reference values denoted by subscript o, so that

$$v^* = \frac{v}{v_o} \qquad x^* = \frac{x}{x_o} \qquad t^* = \frac{t\, v_o}{l_o}$$

$$p^* = \frac{p}{\rho_o v_o^2} \qquad \varphi^* = \frac{\Delta\varphi}{\Delta\varphi_o} \qquad \boldsymbol{E}^* = \frac{\boldsymbol{E}\, l_o}{\Delta\varphi_o}$$

$$q^* = \frac{q}{q_o} \qquad T^* = \frac{\Delta T}{\Delta T_o} \qquad g^* = \frac{g}{g_o} \tag{11}$$

Here, T_c is the temperature of the cold wall and T_h is the temperature of the hot wall, so that $\Delta T = T - T_c$ and $\Delta T_o = T_h - T_c$. Similarly, $\Delta\varphi_o$ is the reference value of the difference of the electric potential between the two electrodes. The following nondimensional groups should be recognized as

Reynolds number	$\mathrm{Re} = \frac{\rho_o v_o l_o}{\eta_o}$
Prandtl number	$\mathrm{Pr} = \frac{c_{po} \eta_o}{k_o}$
Grashof number	$\mathrm{Gr} = \frac{\rho_o^2 g_o \alpha_o \Delta T_o l_o^3}{\eta_o^2}$
Eckert number	$\mathrm{Ec} = \frac{v_o^2}{c_{po} \Delta T_o}$
Froude number	$\mathrm{Fr}^2 = \frac{v_o^2}{g_o l_o}$
Charge diffusivity number	$\mathrm{D_e} = \frac{\eta_o}{\rho_o D_o}$
Lorentz force number	$\mathrm{S_e} = \frac{q_o \Delta\varphi_o}{\rho_o v_o^2}$
Electric Prandtl number	$\mathrm{Pr_e} = \frac{\eta_o}{\rho_o b_o \Delta\varphi_o}$
Electric field number	$\mathrm{N_e} = \frac{q_o l_o^2}{\varepsilon_o \Delta\varphi_o}$

(12)

Fluid density, electric charge mobility and coefficients of specific heat, thermal expansion, viscosity and heat conduction can be expressed as

$$\rho = \rho_o\, \rho'(\theta) \qquad b = b_o\, b'(\theta) \qquad c_p = c_{po}\, c_p'(\theta)$$

$$\alpha = \alpha_o\, \alpha'(\theta) \qquad \eta = \eta_o\, \eta'(\theta) \qquad k = k_o\, k'(\theta) \tag{13}$$

where the primed values denote generalized functions of non-dimensional temperature. The non-dimensional density ρ' can be expanded in Taylor series while retaining only the first order term

$$\rho' = 1 - \alpha\, \Delta T = 1 - \alpha^* \theta \tag{14}$$

where

$$\alpha^* = \frac{\partial \rho'}{\partial \theta} = \frac{\partial \rho'}{\partial \theta} \frac{\Delta T_o\, \rho_o}{\rho_o\, \Delta T_o} = \frac{1}{\rho_o} \frac{\partial \rho}{\partial T} \Delta T_o = \alpha\, \Delta T_o \tag{15}$$

It can be assumed that the coefficient of thermal expansion, α, is constant in the range of temperatures which are of interest in a particular case. When the term $(\alpha\, \Delta T_O) \ll 1$, starting with the complete Navier-Stokes equations for compressible fluid flow, equations more general than what is known as the Boussinesq approximation can be derived[14] for the fluid with non-constant properties. Thus, the system of equations (1-10) for incompressible flow of a fluid with temperature dependent properties and electric charges under the influence of an electric field can be reduced[15] to

$$\nabla^* \cdot v^* = 0 \tag{16}$$

$$\frac{\partial v^*}{\partial t^*} + \nabla^* \cdot (v^*\, v^* + \tilde{p}^*\, I) = \frac{1}{Re} \nabla^* \cdot (\eta'\, \nabla^* v^*) + \frac{Gr\, \theta}{Re^2} g^* + S_e\, q^*\, E^* \tag{17}$$

$$\frac{\partial \theta}{\partial t^*} + \nabla^* \cdot (\theta^*\, v^*) = \frac{1}{Pr\, Re\, c_p} \nabla^* \cdot (k'\, \nabla^* \theta) + \frac{S_e\, Ec}{c_p} [(q^* (v^* + \frac{1}{Re\, Pr_e} E^*) - \frac{1}{Re\, D_e} \nabla^* q^*) \cdot E^* \tag{18}$$

$$\frac{\partial q^*}{\partial t^*} + \nabla^* \cdot \left[q^* (v^* + \frac{1}{Re\, Pr_e} E^*) \right] = \frac{1}{Re} \nabla^* \cdot (\frac{1}{D_e} b' \nabla^* q^*) \tag{19}$$

$$\nabla^{*2} \varphi^* = - N_e\, q^* \tag{20}$$

where $\tilde{p}^* = p^* + \frac{\phi^*}{Fr^2}$ so that $g^* = \nabla^* \phi^*$. It should be pointed out that viscous dissipation is negligible[14,15] since its ratio with respect to the convective term in the energy equation is of the order $\frac{Ec}{Re}$.

3. Numerical model

Based on the mathematical model derived above, a numerical model has been developed. For simplicity and clarity of notation, the asterisk symbol in the system of equations (16-20) will be omitted. The system can be written in fully conservative vector form in physical Cartesian coordinates as follows

$$\frac{\partial Q}{\partial t} + \frac{\partial E}{\partial x} + \frac{\partial F}{\partial y} + \frac{\partial G}{\partial z} = \left[\frac{\partial}{\partial x} \left(D \frac{\partial Q}{\partial x} \right) + \frac{\partial}{\partial y} \left(D \frac{\partial Q}{\partial y} \right) + \frac{\partial}{\partial z} \left(D \frac{\partial Q}{\partial z} \right) \right] + S \tag{21}$$

The solution vector Q is

$$Q = \begin{bmatrix} \tilde{p}/\beta \\ u \\ v \\ w \\ \theta \\ q \end{bmatrix} \tag{22}$$

where $\frac{\partial (\tilde{p}/\beta)}{\partial t}$ represents artificial compressibility[20], and β is the artificial compressibility coefficient. The generalized flux vectors are given by

$$E = \begin{bmatrix} u \\ u^2+\tilde{p} \\ uv \\ uw \\ u\theta \\ q(u+\frac{1}{RePr_e} E_x) \end{bmatrix} \qquad F = \begin{bmatrix} v \\ vu \\ v^2+\tilde{p} \\ vw \\ v\theta \\ q(v+\frac{1}{RePr_e} E_y) \end{bmatrix}$$

$$G = \begin{bmatrix} w \\ wu \\ wv \\ w^2+\tilde{p} \\ w\theta \\ q(w+\frac{1}{RePr_e} E_z) \end{bmatrix} \tag{23}$$

The source term vector S and diagonal matrix D are

$$S=\begin{bmatrix} 0 \\ \frac{Gr}{Re^2}\theta g_x + S_e\, q\, E_x \\ \frac{Gr}{Re^2}\theta g_y + S_e\, q\, E_y \\ \frac{Gr}{Re^2}\theta g_z + S_e\, q\, E_z \\ \frac{S_e\, Ec}{c_p'}\left[q\left(v+\frac{1}{RePr_e}E\right) - \frac{1}{Re\, D_e}\nabla q\right]\cdot E \\ 0 \end{bmatrix}$$

$$D = \frac{1}{Re}\begin{bmatrix} 0 \\ \eta' \\ \eta' \\ \eta' \\ \frac{k'}{Pr\, c_p'} \\ \frac{b'}{D_e} \end{bmatrix}^T \qquad (24)$$

The electric potential field equation (20) is solved separately. The electric field vector $\boldsymbol{E}$ and normal to the wall $\mathbf{n}$ are written in terms of Cartesian coordinates

$$E = (E_x, E_y, E_z)^T$$

$$g = (g_x, g_y, g_z)^T$$

Here, the superscript ^{T} denotes the transposition of a vector. After transformation to generalized curvilinear non-orthogonal coordinates in computational space, the system of governing equations can be written as

$$\frac{\partial \tilde{Q}}{\partial t} + \frac{\partial \tilde{E}}{\partial \xi} + \frac{\partial \tilde{F}}{\partial \eta} + \frac{\partial \tilde{G}}{\partial \zeta} = D^2(J\tilde{Q}) + \tilde{S} \qquad (25)$$

The solution vector, flux and source term vectors in curvilinear coordinates are

$$\tilde{Q}=\frac{1}{J}\begin{bmatrix} \tilde{p}/\beta \\ u \\ v \\ w \\ \theta \\ q \end{bmatrix} \qquad \tilde{E}=\frac{1}{J}\begin{bmatrix} U \\ Uu+\xi_x\tilde{p} \\ Uv \\ Uw \\ U\theta \\ q(U+\frac{1}{RePr_e}E_\xi) \end{bmatrix}$$

$$\tilde{F}=\frac{1}{J}\begin{bmatrix} V \\ Vu \\ Vv+\eta_y\tilde{p} \\ Vw \\ V\theta \\ q(V+\frac{1}{RePr_e}E_\eta) \end{bmatrix} \qquad (26)$$

$$\tilde{G}=\frac{1}{J}\begin{bmatrix} W \\ Wu \\ Wv \\ Ww+\zeta_z\tilde{p} \\ W\theta \\ q(W+\frac{1}{RePr_e}E_\zeta) \end{bmatrix} \qquad (27)$$

$$\tilde{S}=\begin{bmatrix} 0 \\ \frac{Gr}{Re^2}\theta g_\xi + S_e\, q\, E_\xi \\ \frac{Gr}{Re^2}\theta g_\eta + S_e\, q\, E_\eta \\ \frac{Gr}{Re^2}\theta g_\zeta + S_e\, q\, E_\zeta \\ \frac{S_e\, Ec}{c_p'}\left[q\left(v+\frac{1}{RePr_e}E\right) - \frac{1}{Re\, D_e}\nabla q\right]\cdot E \\ 0 \end{bmatrix}$$

$$\tilde{D} = D \qquad D^2(J\tilde{Q}) = \left[\frac{D}{J}g_{ij}\left(J\tilde{Q}\right)_{,j}\right]_{,i} \qquad (28)$$

where $J = \dfrac{\partial(\xi,\eta,\zeta)}{\partial(x,y,z)}$ is the determinant of the Jacobian geometric transformation matrix from physical x,y,z into computational ξ,η,ζ space, and g_{ij} is the metric tensor given by

$$g_{ij} = \nabla x_i' \cdot \nabla x_j' \qquad (29)$$

Contravariant velocity components are related to velocity components in Cartesian coordinate system as follows

$$\begin{bmatrix} U \\ V \\ W \end{bmatrix} = \begin{bmatrix} \xi_x & \xi_y & \xi_z \\ \eta_x & \eta_y & \eta_z \\ \zeta_x & \zeta_y & \zeta_z \end{bmatrix}\begin{bmatrix} u \\ v \\ w \end{bmatrix} \qquad (30)$$

Equation (25) constitutes a system of coupled nonlinear partial differential equations. This system can be solved using a four-stage Runge-Kutta explicit time stepping method[22] given by

$$\tilde{Q}^0 = \tilde{Q}^n$$
$$\Delta\tilde{Q}^m = -\gamma_m \Delta t\ \tilde{R}^{m-1} \quad m = 1,2,3,4$$
$$\tilde{Q}^{n+1} = \tilde{Q}^n + \Delta\tilde{Q}^4 \tag{31}$$

The iteration level is denoted by n, and each stage of the Runge-Kutta method by m, where the coefficients are γ_m = 1/4, 1/3, 1/2 and 1, respectively. The residual $\tilde{R}$ is defined as

$$\tilde{R} = \frac{\partial\tilde{E}}{\partial\xi} + \frac{\partial\tilde{F}}{\partial\eta} + \frac{\partial\tilde{G}}{\partial\zeta} - D^2(J\tilde{Q}) - \tilde{S}$$
$$- \frac{\varepsilon_2\psi}{2J\Delta t}\left[\frac{\partial^2}{\partial\xi^2} + \frac{\partial^2}{\partial\eta^2} + \frac{\partial^2}{\partial\zeta^2}\right](J\tilde{Q})$$
$$- \frac{\varepsilon_4\psi}{8J\Delta t}\left[\frac{\partial^4}{\partial\xi^4} + \frac{\partial^4}{\partial\eta^4} + \frac{\partial^4}{\partial\zeta^4}\right](J\tilde{Q}) \tag{32}$$

A combination of second and fourth order artificial dissipation is necessary in EHD-type problems because of the existence of sharp gradients in the charged particle density distribution. The last two terms in equation (32) represent second and fourth order artificial dissipation[21,22] terms which are added to improve the stability of the scheme and to prevent[15] the electric charge signs from changing locally in the flow field. The artificial dissipation sensor function, ψ, was based on a normalized value of the local gradient of the charge density distribution. The influence of artificial dissipation terms is controlled by ε_2 and ε_4 which are user-specified small parameters. To further enhance the convergence rate, implicit residual smoothing was used. Poisson's equation was solved for the smoothed residual after each stage of the Runge-Kutta iteration.

$$\nabla^2\hat{R}_i = \tilde{R}^m{}_i \tag{33}$$

This equation was discretized and numerically solved by ADI scheme

$$(1 - \omega\delta_{\xi\xi})(1 - \omega\delta_{\eta\eta})(1 - \omega\delta_{\zeta\zeta})\hat{R}_i = \tilde{R}^m{}_i \tag{34}$$

where the smoothing operator is denoted by δ and ω is a user-specified constant, while $\hat{R}_i$ represents the smoothed residual.

4. Boundary conditions

By introducing the artificial compressibility term in the continuity equation, the system of equations becomes hyperbolic. Therefore, boundary conditions have to be applied considering characteristic directions. Proper boundary conditions are determined from the nonconservative form of the transformed system (25)

$$\frac{\partial\tilde{Q}}{\partial t} + \tilde{A}\frac{\partial\tilde{Q}}{\partial\xi} + \tilde{B}\frac{\partial\tilde{Q}}{\partial\eta} + \tilde{C}\frac{\partial\tilde{Q}}{\partial\zeta} = D^2(J\tilde{Q}) + \tilde{S}. \tag{35}$$

The eigenmatrix corresponding to the flux vector Jacobian $\tilde{A}$ is

$$\tilde{\Lambda} = \mathrm{diag}(U-a, U+a, U, U, U, U) \tag{36}$$

where a is an equivalent speed of sound

$$a = \sqrt{U^2 + \beta(\xi_x^2 + \xi_y^2 + \xi_z^2)}. \tag{37}$$

It can be concluded that one of the eigenvalues is negative for the 'subsonic' case. Therefore, five variables must be specified as boundary conditions at the inlet and one variable corresponding to the negative eigenvalue at the exit.

Boundary conditions are imposed by premultiplying the boundary equations by the modal matrix M and thus transforming the system of equations into characteristic form. Furthermore, the equations are premultiplied by a selection matrix L to select the variable which will be computed from the equation. The equation corresponding to the point at the boundary is

$$\left[LM_\xi^{-1} + \frac{\partial\Omega}{\partial\tilde{Q}}\right]\Delta\tilde{Q} = -\gamma_m\Delta t\left[LM_\xi^{-1}\tilde{R}^{m-1} + \frac{\Omega^n}{\gamma_m\Delta t}\right] \tag{38}$$

The selection matrix and the boundary condition vector for the inlet boundary are

$$L = \mathrm{diag}(1,0,0,0,0,0) \tag{39}$$

$$\Omega = (0, u-u_p, v-v_p, w-w_p, \theta-\theta_p, q-q_p)^T \quad (40)$$

The selection matrix and the boundary condition vector for the exit boundary are

$$L = \mathrm{diag}(0,1,1,1,1,1) \quad (41)$$

$$\Omega = (p-p_p, 0,0,0,0,0)^T \quad (42)$$

Wall boundary conditions have the same form as the inlet boundary conditions, except for the pressure which is computed from the normal momentum equation (17) as

$$n \cdot \nabla \tilde{p} = n \cdot \left[\frac{1}{Re} \nabla \cdot (\eta' \nabla v) + \frac{Gr\, \theta}{Re^2} g + S_e\, q\, E \right] \quad (43)$$

Boundary conditions for electric charges on the solid boundaries were of the Neumann type. The Poisson equation for the electric potential (Eq. 10) was solved separately during each global iteration using an ADI algorithm.

An extension of this formulation to include multiple charged species and an electrically non-neutral carrier fluid should be conceptually straightforward, although it would require a substantial increase in computational resources.

5. Computational results

Based on the analytical formulation and the numerical algorithm, a two-dimensional flow analysis computer code was written. The value of the artificial compressibility parameter was $\beta = 10$ in all computer runs. All computations were performed on the Cray-YMP computer at NASA Ames Research Center and postprocessed in our Computational Fluid Dynamics Laboratory at Penn State University.

Two sets of computer runs were performed. The first set consisted of two cases where the two-dimensional flowfield was computed in the plane of the mean flow. The second set consisted of four cases where the two-dimensional flowfield was computed perpendicular to the mean flow.

5.1. Computations in the mean flow plane

The first test case was a simple model for steady flow in a rectangular electrophoresis chamber. A charged fluid was injected at the centerline of the electrically neutral carrier fluid flow. Temperature was constant along the boundaries and Joule's heating and buoyancy force effects were neglected, so that heat transfer effects were not taken into account. Numbers characterizing the flowfield are summarized in Table 1. A computational grid consisting of 60 × 60 nonclustered cells was used to discretize the flow domain having an aspect ratio AR = 10:1 with the mean flow running from left to right. Initially, charges were specified only at the injection point on the left vertical boundary. A fully developed parabolic velocity profile throughout the flowfield and a linear variation of the electric potential between the top and bottom walls were used as initial conditions. A constant electric potential difference was applied at every station across the passage starting from the inlet until a point located at 75 percent of the distance from inlet to exit. Thus, along the top and bottom wall, no electric potential difference was applied between 75 percent and 100 percent of the passage length.

The convergence rate was slow and could be slightly improved by applying implicit residual smoothing. As a consequence of the imposed electric field, the charged fluid was deflected from the centerline as it was carried by the carrier fluid along the chamber. Since the nondimensional charge density at the inlet boundary was specified as smoothly varying over nine grid points (having a value of one at the centerline), the given case represented a difficult task from a numerical point of view. We have attempted to overcome this problem by explicitly adding a small amount of fourth order artificial dissipation. However, it was found that even a very small amount of artificial dissipation necessary to enhance the convergence rate has a detrimental effect on the accurate prediction of the diffusion of charged particles (Fig. 1). To overcome these difficulties and to eliminate high frequency error modes, the charge density was explicitly forced to be non-negative. Results obtained applying this condition seem to be much better, but a new problem has occurred. Charges were not conserved any longer and the convergence rate was again not satisfactory. Consequently, by trial and error, it was found the combined artificial dissipation of second and fourth order with coefficients having values of $\varepsilon_2 = 0.0004$ and $\varepsilon_4 = 0.0005$ gave acceptable results.

Specifically, for the case when the electric potential difference was $\Delta\varphi$ = 70 V, the predicted electric charge density profiles at different stations along the channel (Fig. 2) indicate slight bending and diffusion of the charged particle stream, while accurately preserving global charge conservation at every station (Fig. 3). Figure 4 depicts the monotonic convergence history of the iterative process where the grid point normalized sum of the residuals of the system (Eq. 32) is plotted versus the number of iterations. Figure 5 depicts the predicted stream of charged particles, isobars and the electric potential lines. Notice that the electric potential field is influenced by the presence of the highly concentrated stream of charged particles. Similar results were obtained with an electric potential field difference of $\Delta\varphi$ = 100 V (Fig. 6 and 7) where slightly stronger diffusion and bending of the charged particle stream occurred. If the electric potential field difference is increased significantly, the stream of charged particles can be deflected so that it meets the side wall (Fig. 8). In this case, the spurious negative values of charges (Fig. 9) started to appear. This problem could be treated only by reevaluating the artificial dissipation terms and by increasing the order of accuracy of the numerical implementation of the wall boundary conditions.

5.2. Computations in the cross plane

First, we shall demonstrate an example of the fluid flow generated by the electric field. The mechanism of such an instability can be seen by analogy with the classical Benard problem. Electroconvective vortices[8-10,15] analogous to thermoconvective vortices will be developed if sufficient electrical potential energy can be released by inverting a charged layer. In a closed chamber the charged particles were uniformly injected through the lower wall while treating the top wall as an exit boundary for the charged particles since the side walls had a Neumann condition imposed. An external electric field was imposed by means of electrodes along the lower and the upper wall. In this case, Joule's heating and buoyancy force were taken into account. Nondimensional numbers were Pr=1, Gr=3000, $Re = Gr^{1/2}$, Ec=1, $D_e = \frac{1}{Re}$, S_e=1, N_e=1000, Pr_e=1. Temperature was kept constant along the boundaries and pressure was computed using the normal momentum equation along all four walls. Figure 10 depicts the resulting flow field consisting of two dominant vortices, a second pair of vortices that were elongated and pushed toward walls, and the development of a third pair of vortices near the center of the chamber. Charge density contours are shown in Figure 11 confirming that the boundary conditions were satisfied accurately.

In free flow electrophoretic devices, it is of extreme importance to understand and predict the flow field in planes that are perpendicular to the main flow direction. It is in these planes that the characteristic oval and crescent shapes[11,17,23-25] of the charged particle stream cross sections are observed. They have been attributed solely to electroosmotic effects and the ratio of electric conductivities and electric permitivities of the charged particles and the carrier fluid. In our studies, the carrier fluid was electrically nonconductive and neutrally charged. A series of computational runs was performed where the cross section of an electrophoretic chamber was modelled as a closed container with thermally insulated vertical walls along which the electrodes were located. The top and bottom walls were either kept at the same temperature or had a constant temperature difference of ΔT = 2 K in order to study the effect of a thermally induced buoyancy flow. The aspect ratio of the chamber was AR = 6:1. The chamber was discretized with 180 × 60 grid cells that were smoothly clustered towards the walls and the horizontal and vertical axes of the channel. Initial conditions assumed zero velocity in the entire domain and a linear variation of the electric potential between the vertical walls. A highly concentrated area of electrically charged particles was initially specified over the region occupied by 3 × 3 grid cells located at the geometric center of the chamber. These charged particles were consequently forced to move under the influence of the Lorentz force and thermally induced buoyancy. A summary of all the characteristic flow variables may be found in Table 2.

In the case when the electric potential difference was $\Delta\varphi$ = 70 V and the top and bottom walls were kept at the same temperature, the charged particles moved only slightly from the center while undergoing diffusion and assuming a horizontal elliptic shape (Fig. 11). The Lorentz force effects resulted in the creation of two counter-rotating

vortices positioned above and below the charged particles (Fig. 12).

The next test case involved an electric potential difference of $\Delta\varphi$ = 200 V, while keeping all other parameters the same (Table 2). In this case, the bottom wall was kept at a uniform temperature that was 2 K higher than the uniform temperature of the upper wall. The electric charges moved significantly (Fig. 13) and formed a characteristic wedge shape. From the same figure, it can be concluded that the opening of the wedge is enhanced by the locally vertical velocity components due to recirculation. It should also be noted that the recirculation intensity increases towards the vertical side walls representing the electrodes.

When the electric potential difference was increased to $\Delta\varphi$ = 700 V, the charges were removed from the entire field and deposited on the electrode represented by the right side vertical wall. A very strong recirculation pattern predicted in this case (Fig. 14) is reminiscent of the thermal buoyancy due to Joule heating as caused by a strong external magnetic field.

In order to simulate a somewhat more realistic configuration, the aspect ratio of the chamber was increased to AR = 20:1 while keeping the same number of grid cells and all other parameters the same (Table 2). In the case when $\Delta\varphi$ = 400 V, the initially circular charge density pattern transformed into a diffused and shifted arrow shape. Recirculation was strong only close to the electrodes (Fig. 15). When $\Delta\varphi$ = 700 V, the electric charges' domain was stretched until it reached the right electrode. The recirculation pattern was similarly nonexistent except next to the electrodes (Fig. 16). These test cases converged smoothly although they took significantly longer to converge because of the increased distance between the electrodes and the initial location of the charged particles.

Conclusions

An electrohydrodynamic flow model has been developed and computations including thermally and electrically induced motion have been performed using a finite difference method. It has been found that artificial dissipation causes excessive diffusion of charged particles and influences the convergence rate of the iterative process. The existence of cross plane electroconvective vortices analogous to thermoconvective vortices has been computationally demonstrated. Diffusion and convection of charged particles under the influence of a steady electric field has resulted in patterns that have been documented in literature. An extension of this work to a fully three-dimensional software package which will include a multi-species environment, a magnetic field and time-dependent processes is in progress.

Acknowledgments

The lead author expresses his gratitude to the Center for Cell Research at the Pennsylvania State University for support during his tenure as a post-doctoral fellow. The authors are grateful to Dr. Robert Stubbs of NASA Lewis Research Center for providing the computing time on NAS facility. Special thanks are due to Dr. D. Saville, Dr. C. Ivory, Dr P. Rhodes, Dr. R. Snyder and Dr. M. Zahn for helpful discussions and copies of their publications and to Mr. Scott Sheffer for his generous help in the preparation of the final paper. Graphics was performed on computing equipment donated by Apple Computer, Inc.

References

1. Stuetzer, O. M., "Magnetohydrodynamics and Electrohydrodynamics," The Physics of Fluids, Vol. 5, No. 5, May 1962, pp. 534-544.
2. Lee, S. and Dulikravich, G. S., "Magnetohydrodynamic Flow Computations in Three Dimensions", AIAA Paper 91-0388, Reno, NV, Jan. 1991a, also in International Journal for Numerical Methods in Fluids, summer 1991.
3. Lee, S. and Dulikravich, G. S., "Computation of Magnetohydrodynamic Flow With Joule Heating and Buoyancy", Proceedings of International Aerospace Congress, Melbourne, Australia, May 13-17, 1991.
4. Dulikravich, G. S., Kosovic, B. and Lee, S., "Solidification of Variable Property Melts in Closed Containers: Magnetic Field Effects," Proc. 13th IMACS World Congress on Computation and Applied Math., Dublin, Ireland, July 22-26, 1991.
5. Landau, L. D. and Lifshitz, E. M., Electrodynamics of Continuous Media, Pergamon Press, New York, 1960.

6. Melcher, J. R., Continuum Electromechanics, The MIT Press, Cambridge, 1981.
7. Babskii, V. G., Zhukov, M. Y. and Yudovich, V. I., "Mathematical Theory of Electrophoresis," (translated by C. Flick), Consultants Bureau, New York, 1989.
8. Eringen, A. C., and Maugin, G. A., Electrodynamics of Continua I: Foundations and Solid Media, Springer-Verlag, New York, 1990.
9. Eringen, A. C., and Maugin, G. A., Electrodynamics of Continua II: Fluids and Complex Media, Springer-Verlag, New York, 1990.
10. Ostroumov, G. A., "Electric Convection," Inzhenerno-Fizicheskii Zhurnal, Vol. 10, No. 5, 1966, pp. 683-695.
11. Saville, D. A., "The Fluid Mechanics of Continuous Flow Electrophoresis in Perspective", PhysicoChemical Hydrodynamics, Vol. 1, 1980, pp 297-307.
12. Ivory, C. F., Gobie, W. A., Bekwith, J. B., Hergenrother, R. and Malec, M., "Electromagnetic Stabilization of Weakly Conducting Fluids", Science, Vol. 238, Oct. 1987, pp. 58-61.
13. Mazhorova, O. S., Popov, Y. P. Pokhilko, V. I. and Feonychev, A. I., "Numerical Investigation of Liquid Electrophoresis Without Support Media," Izvestia Academii Nauk SSSR, Mekhanika Zhidkosti i Gaza, No. 3, May-June 1988, pp. 14-20.
14. Gray, D. D., and Giorgini, A., "The Validity of the Bousinessq Approximation for Liquids and Gases," International Journal of Heat and Mass Transfer, Vol. 19, 1976, pp. 545-551.
15. Lee, S., Dulikravich, G. S.and Kosovic, B., "Computer Simulation of Electrophoretic Separation Processes," Proc. 17th Annual Northeast Bioeng. Conference, University of Connecticut, Hartford, CT, April 4-5, 1991.
16. Biscans, B., Hennequin, J. C., Bertrand, J., "Some Aspects of Continuous Flow Electrophoresis in Microgravity", Acta Astronautica, Vol. 13, No. 11/12, 1986, pp. 705-713.
17. Changeart, J. F., Marsal, O., Sanchez, V., Zager, F., Costet, R. and Armadieu, P., "SELECTE: Scientific Instrument Devoted to Continuous Flow Electrophoretic Separation on Earth and in Space," Proc. of 6th European Symposium of Material Sciences Under Microgravity Conditions, Bordeaux, France, Dec. 2-5. 1986, pp. 285-290; also ESA SP-256, Feb. 1987.
18. Hamano, N., Mitami, K., Tsubouchi, K., Takagi, Y., Okusawa, T., Wakasugi, N., Shimbo, C. and Sakai, H., "Development of Electrophoresis Equipment for SFU," Proceedings of the 16th International Symposium on Space Technology and Science, Sapporo, Japan, Vol. 2, 1988, pp. 2459-2464.
19. Bello, M. S. and Polezhaev, V. I., "Hydrodynamics, Gravitational Sensitivity and Transport Phenomena in Continuous Flow Electrophoresis," AIAA paper 91-0112, Aerospace Sciences Meeting, Reno, NV, Jan. 7-10, 1991.
20. Chorin, A. J., "A Numerical Method for Solving Incompressible Viscous Flow Problems," Journal of Computational Physics, Vol. 2, 1967, pp. 12-26.
21. Jameson, A., Schmidt, W., and Turkel, E., "Numerical Solutions of the Euler Equations by Finite Volume Methods Using Runge-Kutta Time-Stepping Scheme," AIAA paper 81-1259, Palo Alto, CA, June, 1981.
22. Steger, J. L. and Kutler, P., "Implicit Finite-Difference Procedure for the Computation of Vortex Wakes," AIAA Journal, Vol. 15, No. 7, July 1977, pp. 581-590.
23. Rhodes, H. P. and Snyder, R. S., "Preparative Electrophoresis for Space", NASA TP 2777, 1987.
24. Ivory, C., "Continuous Flow Electrophoresis: The Crescent Phenomena Revisited," Journal of Chromatography, Vol. 195, 1980, pp. 165-179.
25. Rhodes, H. P., Snyder, R. S. and Roberts, G. O., "Electrohydrodynamic Distortion of Sample Streams in Continuous Flow Electrophoresis," Journal of Colloid and Interface Science, Vol. 129, No. 1, April 1989, pp. 78-90.

$\Delta\varphi$(V)	Re	Ec	S_e	D_e	Pr_e	N_e
70	400	8.6×10^{-9}	5.83×10^{-3}	2.5×10^{7}	0.2860	25.21
100	400	8.6×10^{-9}	8.3×10^{-3}	2.5×10^{7}	0.2004	17.64
500	400	8.6×10^{-9}	4.16×10^{-2}	2.5×10^{7}	0.0400	3.53

Table 1. Input parameters for AR = 10:1 electrophoretic channel.

$\Delta\varphi$(V)	Re	Ec	S_e	D_e	Pr_e	N_e	Gr
70	9	1.28×10^{-9}	1.067×10^{-2}	1.11×10^{9}	0.2860	100.84	81
200	9	1.28×10^{-9}	3.048×10^{-2}	1.11×10^{9}	0.1002	35.290	81
400	9	1.28×10^{-9}	6.096×10^{-2}	1.11×10^{9}	0.0500	17.145	81
700	9	1.28×10^{-9}	1.067×10^{-1}	1.11×10^{9}	0.0286	10.084	81

Table 2. Input parameters for AR = 6:1 and AR = 20:1 closed chambers.

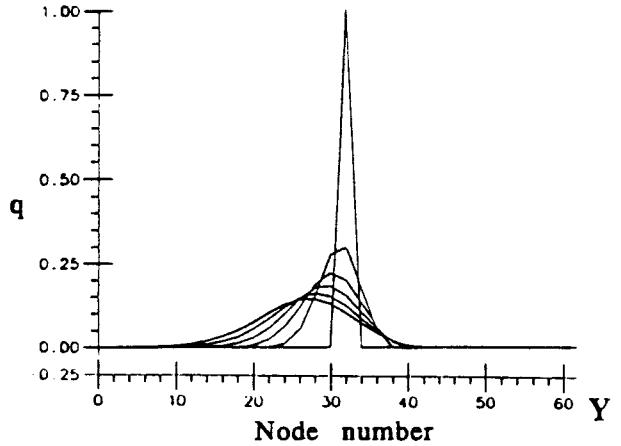

Fig. 1 Artificial dissipation in the numerical algorithm causes excessive diffusion of a charged particle stream injected at the left boundary of an electrophoretic channel.

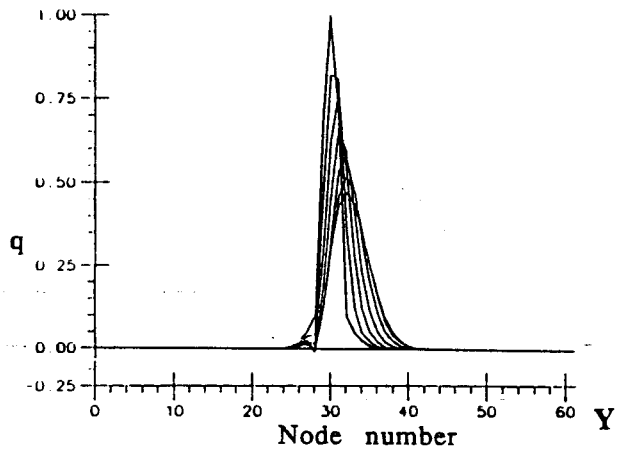

Fig. 2 An EHD channel with AR = 10:1. Electric charge density profiles at successive cross sections after 20 000 iterations with $\Delta\varphi$ = 70 V. Combination of a small amount of second and fourth order artificial dissipation was used resulting in a physically diffusing and shifting profile.

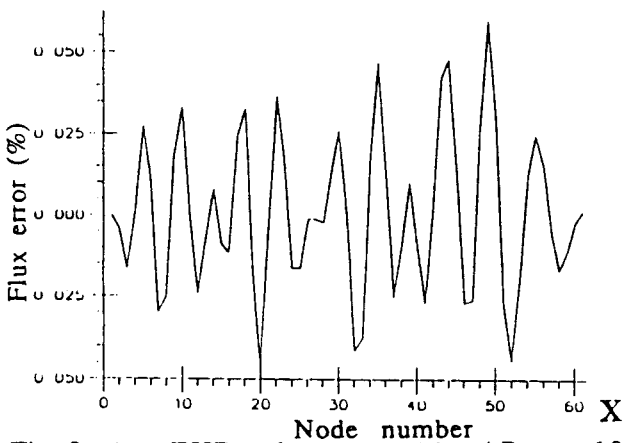

Fig. 3 An EHD channel with AR = 10:1. Percentages of the local normalized error in the integrated electric charge profiles at the successive sections after 20 000 iterations with $\Delta\varphi$ = 70 V.

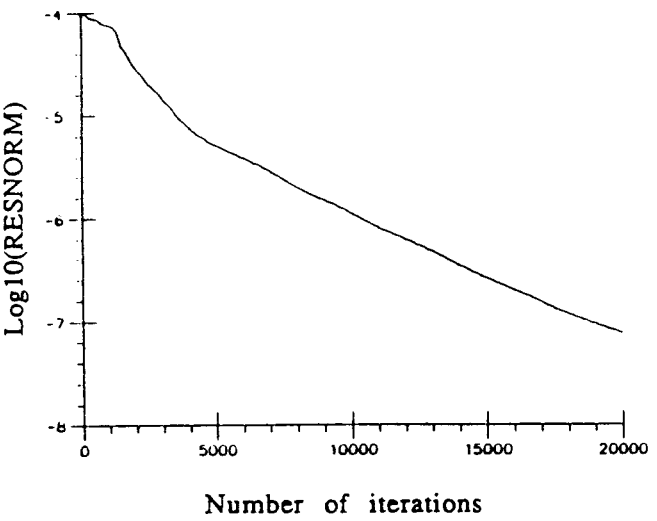

Fig. 4 An EHD channel with AR = 10:1. Convergence history for the case with $\Delta\varphi$ = 70 V.

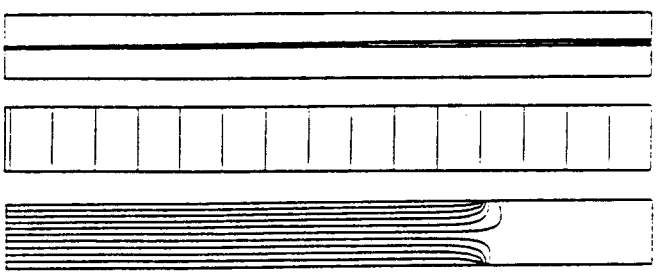

Fig. 5 An EHD channel with AR = 10:1. Electric charge density distribution, constant pressure lines, and constant electric potential lines after 20 000 iterations with $\Delta\varphi$ = 70 V.

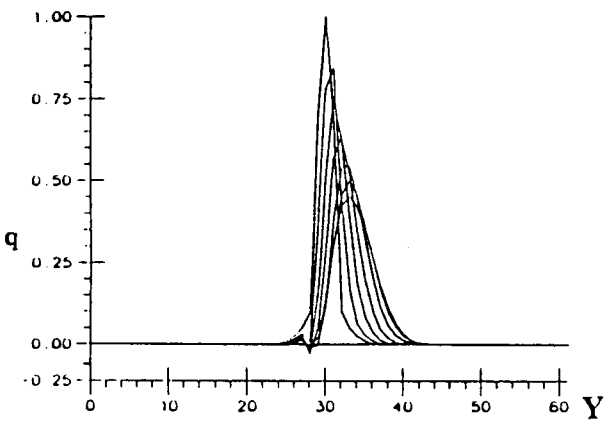

Fig. 6 An EHD channel with AR = 10:1. Electric charge density profiles at successive cross sections after 20 000 iterations with $\Delta\varphi$ = 100 V. Notice a small amount of negative charges been created although a combination of a small amount of second and fourth order artificial dissipation was used.

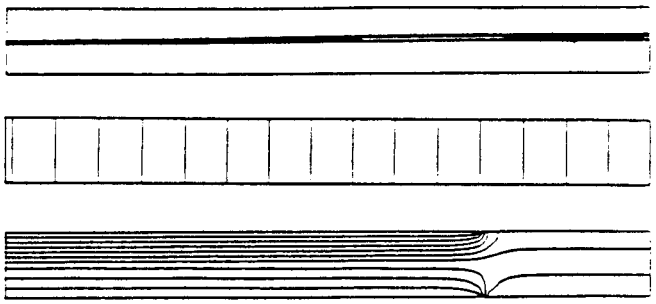

Fig. 7 An EHD channel with AR = 10:1. Electric charge density distribution, constant pressure lines, and constant electric potential lines after 20 000 iterations with $\Delta\varphi$ = 100 V.

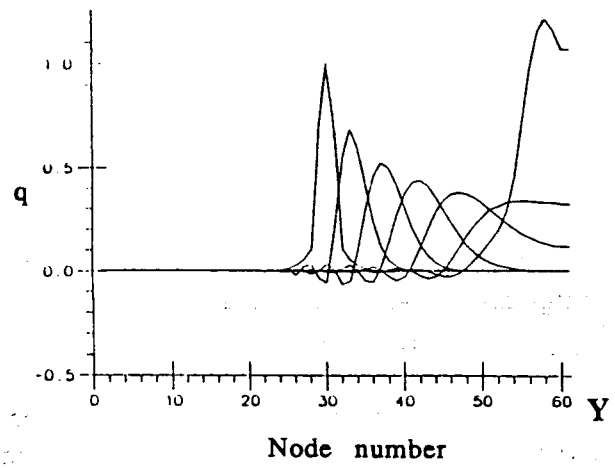

Fig. 8 An EHD channel with AR = 10:1. Electric charge density profiles at successive cross sections after 20 000 iterations with $\Delta\varphi$ = 500 V. Notice a larger amount of negative charges predicted although a combination of a small amount of second and fourth order artificial dissipation was used.

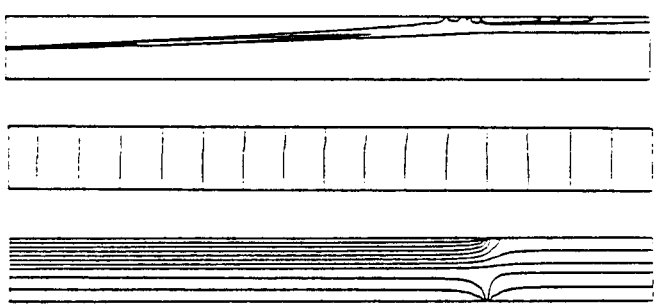

Fig. 9 An EHD channel with AR = 10:1. Electric charge density distribution, constant pressure lines, and constant electric potential lines after 20 000 iterations with $\Delta\varphi$ = 500 V.

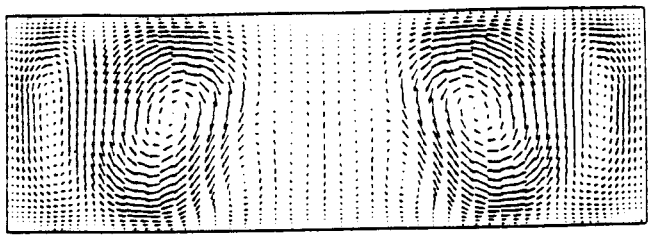

Fig.10 A closed container with AR = 6:1. Strong electroconvective motion created by an electric potential field between top and bottom walls. The container is filled with an electrically conducting fluid and has isothermal walls. Electric charges are uniformly injected at the bottom wall.

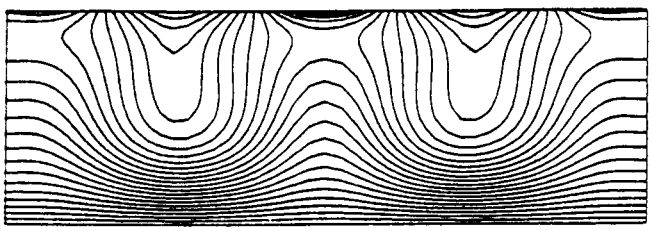

Fig.11 Computed charge density contours for the example in Fig. 10.

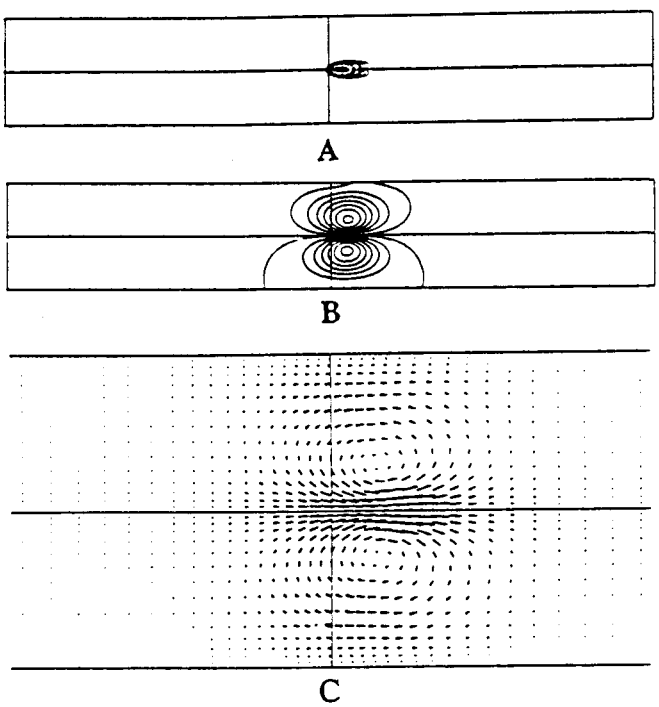

Fig.12 A closed container with AR = 6:1 and $\Delta\varphi$ = 70 V between the vertical walls and ΔT = 2 K between the horizontal walls: a) electric charge density distribution, b) induced streamline pattern, and c) an elarged detail of the velocity vector pattern. The charge pattern is a slightly diffused ellipse.

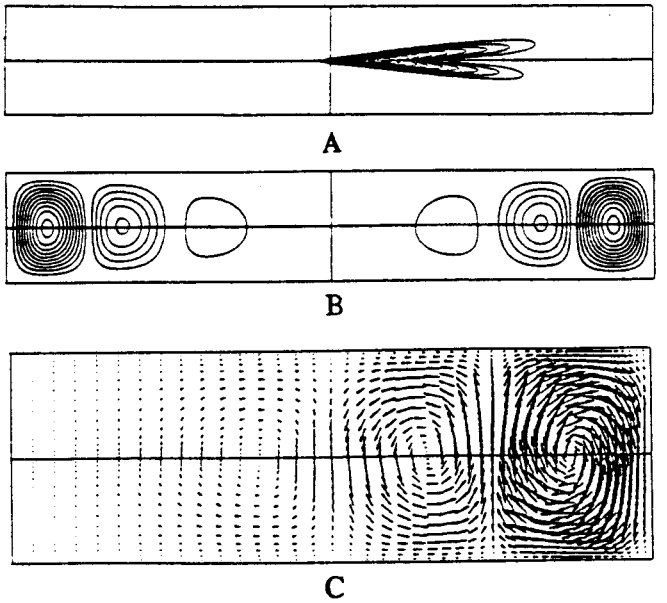

Fig.13 A closed container with AR = 6:1 and Δ = 200 V between the vertical walls and ΔT = 2 K between the horizontal walls: a) electric charge density distribution, b) induced streamline pattern, and c) an elarged detail of the velocity vector pattern. The charge pattern is an arrow shape.

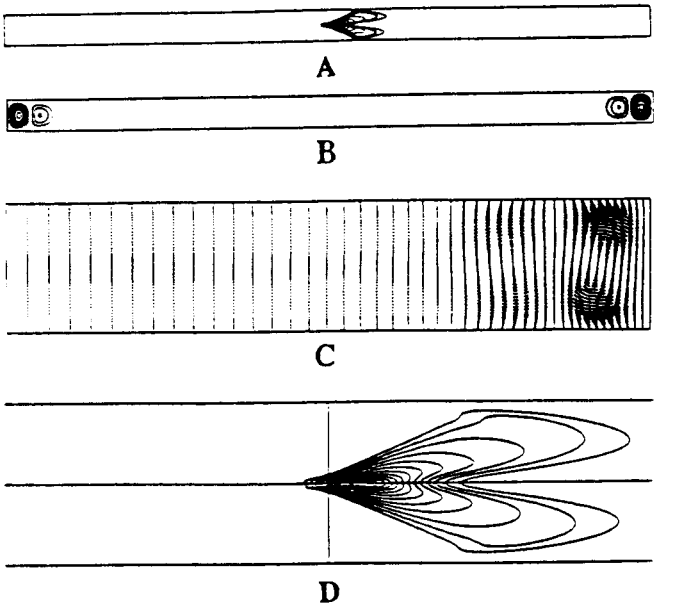

Fig.15 A closed container with AR = 20:1 and Δφ = 400 V between the vertical walls and ΔT = 2 K between the horizontal walls: a) electric charge density distribution, b) induced streamline pattern, c) an elarged detail of the velocity vector pattern, and d) enlarged detail of the charge density pattern.

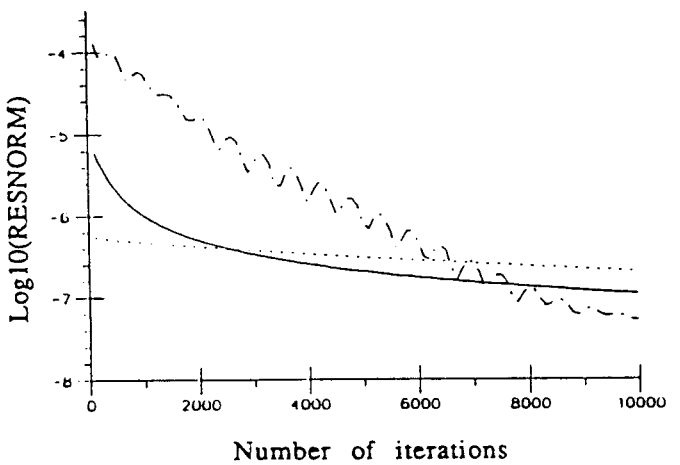

Fig.14 Convergence histories for the AR = 6:1 chamber with ΔT = 2 K between the horizontal walls: Δφ = 70 V (----), Δφ = 200 V (- - -), Δφ = 700 V (- · -).

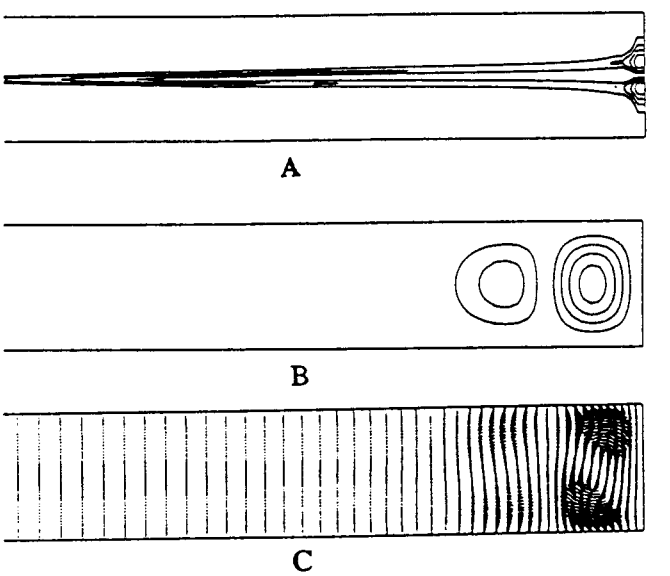

Fig.16 A closed container with AR = 20:1 and Δφ = 700 V between the vertical walls and ΔT = 2 K between the horizontal walls. Details of: a) electric charge density distribution, b) induced streamline pattern, and c) velocity vector pattern.